Effect of yttria inclusion on room temperature tensile properties of investment cast TiAl

Lin, Bochao; Liu, Renci; Jia, Qing; Cui, Yuyou; Withey, Paul A.; Yang, Rui

DOI:
10.1016/j.msea.2017.11.100

Document Version
Peer reviewed version

Citation for published version (Harvard):
Lin, B, Liu, R, Jia, Q, Cui, Y, Withey, PA & Yang, R 2018, 'Effect of yttria inclusion on room temperature tensile properties of investment cast TiAl', *Materials Science and Engineering A*, vol. 712, pp. 73-79. https://doi.org/10.1016/j.msea.2017.11.100

Effect of yttria inclusion on room temperature tensile properties of investment cast TiAl

Bochao Lin, Renci Liu, Qing Jia, Yuyou Cui, Paul A. Withey, Rui Yang

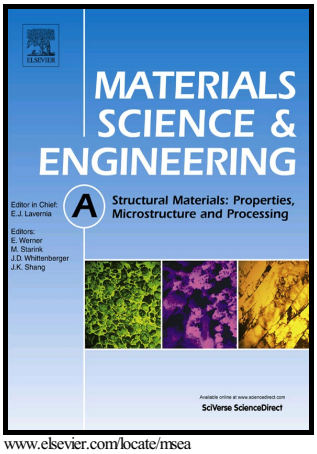

www.elsevier.com/locate/msea

PII: S0921-5093(17)31561-7
DOI: https://doi.org/10.1016/j.msea.2017.11.100
Reference: MSA35815

To appear in: *Materials Science & Engineering A*

Received date: 26 September 2017
Revised date: 24 November 2017
Accepted date: 24 November 2017

Cite this article as: Bochao Lin, Renci Liu, Qing Jia, Yuyou Cui, Paul A. Withey and Rui Yang, Effect of yttria inclusion on room temperature tensile properties of investment cast TiAl, *Materials Science & Engineering A*, https://doi.org/10.1016/j.msea.2017.11.100

Effect of yttria inclusion on room temperature tensile properties of investment cast TiAl

Bochao Lin [1,2], Renci Liu [1], Qing Jia [1], Yuyou Cui [1], Paul A. Withey [3,4], Rui Yang [1]

1. Institute of Metal Research, Chinese Academy of Sciences, 72 Wenhua Road, Shenyang 110016, China.

2. University of Chinese Academy of Sciences, 19(A) Yuquan Road, Beijing, China.

3. Rolls-Royce plc, Derby, DE24 8BJ, UK.

4. School of Metallurgy and Materials, Univerisity of Birmingham, Edgbaston, Birmingham B15 2TT, UK.

Abstract

Yttria is the best face coat material in the shell mold for the investment casting of γ-TiAl alloys. However, yttria inclusions may occur in the cast products and there is a lack of knowledge about the influence of yttria inclusions on the mechanical properties of TiAl. In the present study, the effect of yttria inclusions on room temperature tensile properties of two investment cast TiAl alloys, Ti-45Al-2Mn-2Nb (at.%) + 0.08 vol.% TiB_2 and Ti-46 Al-2 Nb-2Cr-0.15B (at.%), were studied. The results show that tensile failure tends to initiate from yttria inclusions, resulting in reduced plastic strain and ultimate strength. Yttria inclusions differ in location (surface / internal), size, and morphology (agglomerate / whole piece), those with larger sizes or located at the sample surface being more harmful. The tensile properties of inclusion containing TiAl parts can be estimated using the size and location determined by X-ray inspection. The critical size at which inclusions become detrimental to the mechanical properties of TiAl was discussed.

Keywords: TiAl, investment casting, yttria inclusion, tensile properties

1. Introduction

TiAl based alloys are light-weight structural materials with excellent high-temperature performance. Due to reduced component weight and increased fuel efficiency, TiAl based alloys show great potential in fields such as the aerospace and automobile industries [1, 2]. Components including low pressure turbine (LPT) blades, turbine wheels [3] and exhaust valves [4] are now being produced with TiAl alloys.

Investment casting is the most cost-effective method of producing near-net-shape TiAl components [5, 6], and ceramic shell mold production is one of the key steps in the casting route [7]. As TiAl melts are highly reactive, the face coat of the mold is required to be highly inert. Much research has been done on face coat materials and

yttria turns out to be the best option [8-12]. Sintering of yttria is very demanding, and at least 1700°C is needed in order to get a relative high density [13]. However, high sintering temperature will raise cost and, more importantly, the mold will be too hard to deform in the cooling process subsequent to casting, which may cause cracking of the cast products. Therefore an intermediate sintering temperature (1000~1400°C) is usually preferred. Nevertheless, this will result in weaker bonding between yttria particles, and the loose particles may be washed off the mold, swept into the molten metal and become yttria inclusions in the cast products [12, 14]. The detrimental effects of nonmetallic inclusions on mechanical properties of steels and superalloys have been extensively reported [15, 16], while similar effects on TiAl remain unknown. In addition, ductility of TiAl at room temperature is poor and has low repeatability, which restrict its more extensive application [17]. Therefore evaluating the effect of yttria inclusions on the mechanical properties of TiAl is of much importance. In this work, test bars of two typical TiAl based alloys for manufacturing low pressure turbine blades (i.e. 45XD by Rolls-Royce and 4622 based on 4822 by GE) were produced by investment casting using yttria face-coated molds, and room temperature tensile properties of the inclusion containing alloys were investigated; the effects of yttria inclusion size, location and morphology were discussed.

2. Materials and experiments

2.1 Materials and processing

The TiAl alloys used in this study were two typical alloys, Ti-45Al-2Mn-2Nb (at.%) + 0.08 vol.% TiB_2 (45XD) and Ti-46Al-2Nb-2Cr-0.15B (at.%) (4622). Ingots produced with twice VAR (vacuum arc melting) were remelted by ISM (induction skull melting) and centrifugal cast into a mold with an yttria face coat, producing test bars 16 mm in diameter and 210 mm in length. Table 1 shows chemical compositions of the cast rods. The cast rods were hot isostatic pressed (HIPed) at 1260°C and 150 MPa for 4 hours. Heat-treatment was conducted at 1000°C for 4 hours followed by furnace cooling.

2.2 Tensile test

The HIPed and heat treated alloys were machined into tensile samples with a gauge diameter of 5 mm and a gauge length of 25 mm. 50 samples of 45XD and 30 samples of 4622 were tested. All the samples were electropolished in order to eliminate machining marks.

Tensile tests were conducted at room temperature. Plastic strain was measured with an extensometer at a strain rate of $3 \times 10^{-4}\,s^{-1}$ before yielding and $1.6 \times 10^{-3}\,s^{-1}$ after yielding.

2.3 Microstructure studies

The metallographic structures of the heat treated alloys were examined using optical microscopy. The samples were etched by modified Kroll's reagent (5% HF, 10% HNO_3 and 85% H_2O).

Before tensile testing, traditional 2D X-ray imaging with a resolution of about 100 μm was conducted on all the samples as a preliminary detection method for inclusions. Then two samples, one with inclusions detected and one without, were subjected to 3D high resolution X-ray tomography (XRT) on an Xradia VersaXRM-500 3D X-Ray microscope, the detection range being 5 mm in length and 5 mm in diameter from the gauge section of the tensile samples.

After tensile testing, the fracture surfaces were examined on a Shimadzu SSX-550 scanning electron microscope (SEM). Methods including secondary electron imaging (SE), back scattered electron imaging (BSE) and energy dispersive spectroscopy (EDS) were used for inclusion characterization.

3. Results

Microstructures of the two alloys after heat treatment are shown in Fig. 1. 45XD has a fully lamellar microstructure with an average grain (lamellar colony) size of about 70 μm, and few equiaxed gamma grains were observed. Microstructure of 4622 is nearly lamellar, the grain size is similar to 45XD, but contains some equiaxed gamma grains at grain boundaries.

3.1 3D high resolution X-ray tomography

3D high resolution X-ray tomography results are shown in Fig. 2. In addition to the large inclusion detected with traditional X-ray inspection (which caused tensile failure in the subsequent tensile test), more inclusions were observed and most of them are smaller than 60 μm (equivalent spherical diameter).

3.2 Tensile properties

Tensile test results of all the 45XD and 4622 samples are summarized in Table 2. 3 samples exhibited brittle fracture (plastic strain < 0.2%), with no yield strength obtained. For 45XD, yield strength is between 509 MPa and 544 MPa, ultimate strength is between 505 MPa and 681 MPa and plastic strain is between 0.10% and 1.71%. For 4622, yield strength is between 477 MPa and 508 MPa, ultimate strength is between 464 MPa and 601 MPa and plastic strain is between 0.08% and 1.56%. For both alloys, ultimate strength and plastic strain are more scattered than yield strength, and typical strain-stress curves (Fig.3) show that the stress-strain behavior of the samples with varying tensile properties are similar before fracture.

3.3 Fracture surface observation

Both 45XD and 4622 exhibit mostly translamellar fracture and their fracture surfaces are similar. Fig. 4 shows typical fracture surfaces. For samples with good tensile properties (higher ultimate strength and plastic strain, Fig. 4a), no defect was observed on the fracture surfaces. For samples with relatively poor tensile properties (lower ultimate strength and plastic strain), however, cracks were found to initiate from yttria inclusions (Fig. 4b, 4c, 4d) or in some cases from lamellae that are oriented

nearly perpendicular to the loading axis (Fig. 4e, 4f).

4. Discussion

4.1 Characterization of yttria inclusions and their effects on tensile properties

Samples failed from yttria inclusions usually exhibited inferior tensile properties (lower ultimate strength and plastic strain). The crack initiating yttria inclusions differ in size, location and morphology (Fig. 5). Fig. 6 shows the tensile properties of the alloys containing inclusions of different location and morphology plotted against inclusion size. For comparison, tensile properties of samples without yttria inclusion observed on fracture surface are also listed (samples which failed from facets are not included). Different inclusions have different effect on tensile properties. Inclusions located at the sample surface are evidently more harmful than the internal ones. Inclusion size is also important, with plastic strain and ultimate strength decreasing with increasing inclusion size. The influence of inclusion shape is uncertain since there are only 2 samples with whole piece inclusions and their tensile properties are close to samples with agglomerate inclusions of similar location and size. Data in Fig. 6 is a helpful prediction of the tensile properties of inclusion containing TiAl parts, as the inclusion size and location can be determined with non-destructive X-ray inspection.

Mismatch of thermal expansion coefficients and Young's moduli between inclusion (yttria particles) and matrix (TiAl) leads to a tensile stress around inclusions [18] as well as uncoordinated deformation under loading. Strain will concentrate either inside the inclusion or at the matrix/ inclusion interface, resulting in crack initiation inside the inclusion (yttria particles were observed on both halves of the sample, confirming this cracking of yttria inclusions). Tensile failure in titanium and TiAl alloys have been found to initiate from cracked boride participates [19], α particles [20] and lamellae with specific orientation (Fig. 4e, 4f). In these cases, cracks can initiate before plastic strain reaches 0.2% [21]. Due to the low toughness of TiAl, cracks will propagate rapidly when load reaches the critical value. Therefore, tensile properties of TiAl are strongly influenced by these cracks. The detrimental effect of a crack can be quantified by the stress concentration it generated. The maximum stress intensity factor caused by a crack, K_{Imax}, is given approximately by [22]:

$$K_{Imax} = 0.5\sigma_0\sqrt{\pi\sqrt{area}} \quad (1)$$

for an internal inclusion, and by:

$$K_{Imax} = 0.65\sigma_0\sqrt{\pi\sqrt{area}} \quad (2)$$

for a surface inclusion. Here σ_0 is the tensile stress and 'area' is the area of the inclusion on fracture surface. As shown in equations (1) and (2), the K_{Imax} caused by surface and larger inclusions are higher than those of internal and smaller inclusions, which explains why larger and surface inclusions lead to worse tensile properties.

4.2 Critical inclusion size

The crack initiating inclusions observed are usually hundreds of microns in size and the smallest one is 70 μm (converted to equivalent diameter from square root of area, Fig. 2). However, X-ray tomography results suggest that most of the inclusions are smaller than 60 μm (Fig. 2), and these small inclusions were also found in the samples that did not fail from inclusions (such as 4622-11). This indicates the existence of a critical size below which yttria inclusions do not influence the tensile properties of TiAl. The smallest crack initiating inclusion size, 70 μm, is close to the grain size. The work of Nazmy et al. obtained similar results: surface cracks smaller than lamellar grain size have no influence on high cycle fatigue life of TiAl [23]. Moreover, the rogue grains or 'facets' mentioned previously are also larger than the average grain size. These results suggest that a brittle object, whether it is a nonmetallic inclusion, a boride particle, a notch, a cluster of small grains or one single grain with specific lamellar orientation, is harmful to the mechanical properties of TiAl only when it is larger than the grain size. Therefore control of inclusion should be focused on decreasing the size of the largest inclusion and this can be achieved through optimizing mold making technology.

Property consistency and predictability is crucial for safety-critical parts such as turbine blades. As yttria inclusions are inevitable in investment cast TiAl parts, establishment of inclusion-related quality specifications is indispensable and the results in this research provide a reference.

5. Conclusion

Yttria inclusions introduced into TiAl parts during the investment casting process tend to act as crack initiation sites and are detrimental to the room temperature tensile properties of the parts, especially ultimate strength and plastic strain. The effects of yttria inclusions are mainly determined by inclusion location and size. Those located at the sample surface or with larger sizes are more detrimental as they cause a higher stress intensity. The room temperature tensile properties of TiAl can be estimated with inclusion size and location determined by X-ray tomography. The critical inclusion size to cause tensile failure is close to the grain size.

References

[1] Y.-W. Kim, "Intermetallic alloys based on gamma titanium aluminide," *JOM,* vol. 41, pp. 24-30, 1989/07/01 1989.

[2] E. A. Loria, "Gamma titanium aluminides as prospective structural materials," *Intermetallics,* vol. 8, pp. 1339-1345, 9// 2000.

[3] T. Tetsui, "Application of TiAl in a Turbocharger for Passenger Vehicles," *Advanced Engineering Materials,* vol. 3, pp. 307-310, 2001.

[4] K. Gebauer, "Performance, tolerance and cost of TiAl passenger car valves," *Intermetallics,* vol. 14, pp. 355-360, 4// 2006.

[5] F. Appel, J. D. H. Paul, and M. Oehring, *Gamma titanium aluminide alloys: science and technology*: John Wiley & Sons, 2011.

[6] S.-Y. Sung and Y.-J. Kim, "Alpha-case formation mechanism on titanium investment castings," *Materials Science and Engineering: A,* vol. 405, pp. 173-177, 9/25/ 2005.

[7] J. Aguilar, A. Schievenbusch, and O. Kättlitz, "Investment casting technology for production of TiAl low pressure turbine blades – Process engineering and parameter analysis," *Intermetallics,* vol. 19, pp. 757-761, 2011/06/01/ 2011.

[8] J. Kuang, R. Harding, and J. Campbell, "Investigation into refractories as crucible and mould materials for melting and casting γ-TiAl alloys," *Materials Science and Technology,* vol. 16, pp. 1007-1016, 2000.

[9] Q. Jia, Y. Y. Cui, and R. Yang, "A study of two refractories as mould materials for investment casting TiAl based alloys," *Journal of Materials Science,* vol. 41, pp. 3045-3049, 2006/05/01 2006.

[10] R. Yang, Y. Y. Cui, L. M. Dong, and Q. Jia, "Alloy development and shell mould casting of gamma TiAl," *Journal of Materials Processing Technology,* vol. 135, pp. 179-188, 4/20/ 2003.

[11] R. L. Saha, T. K. Nandy, R. D. K. Misra, and K. T. Jacob, "On the evaluation of stability of rare earth oxides as face coats for investment casting of titanium," *Metallurgical Transactions B,* vol. 21, pp. 559-566, 1990/06/01 1990.

[12] R. J. Cui, X. X. Tang, M. Gao, H. Zhang, and S. K. Gong, "Microstructure and composition of cast Ti–47Al–2Cr–2Nb alloys produced by yttria crucibles," *Materials Science and Engineering: A,* vol. 541, pp. 14-21, 4/15/ 2012.

[13] Y. Huang, D. Jiang, J. Zhang, and Q. Lin, "Fabrication of Transparent Lanthanum-Doped Yttria Ceramics by Combination of Two-Step Sintering and Vacuum Sintering," *Journal of the American Ceramic Society,* vol. 92, pp. 2883-2887, 2009.

[14] C. Renjie, G. Ming, Z. Hu, and G. Shengkai, "Interactions between TiAl alloys and yttria refractory material in casting process," *Journal of Materials Processing Technology,* vol. 210, pp. 1190-1196, 6/19/ 2010.

[15] S. Li, "Effects of inclusions on very high cycle fatigue properties of high strength steels," *International Materials Reviews,* vol. 57, pp. 92-114, 2012.

[16] Q. G. Wang, D. Apelian, and D. A. Lados, "Fatigue behavior of A356-T6 aluminum cast alloys. Part I. Effect of casting defects," *Journal of Light Metals,* vol. 1, pp. 73-84, 2// 2001.

[17] A. Lasalmonie, "Intermetallics: Why is it so difficult to introduce them in gas turbine engines?," *Intermetallics,* vol. 14, pp. 1123-1129, 10// 2006.

[18] Y. Murakami, "Chapter 7 - Bearing Steels," in *Metal Fatigue*, Y. Murakami, Ed., ed

Oxford: Elsevier Science Ltd, 2002, pp. 129-162.

[19] D. Hu, "Effect of boron addition on tensile ductility in lamellar TiAl alloys," Intermetallics, vol. 10, pp. 851-858, 2002/09/01/ 2002.

[20] I. Bantounas, D. Dye, and T. C. Lindley, "The role of microtexture on the faceted fracture morphology in Ti–6Al–4V subjected to high-cycle fatigue," Acta Materialia, vol. 58, pp. 3908-3918, 2010/06/01/ 2010.

[21] R. Botten, X. Wu, D. Hu, and M. H. Loretto, "The significance of acoustic emission during stressing of TiAl-based alloys. Part I: Detection of cracking during loading up in tension," Acta Materialia, vol. 49, pp. 1687-1691, 2001/06/13/ 2001.

[22] Y. Murakami, "Chapter 2 - Stress Concentration," in *Metal Fatigue*, Y. Murakami, Ed., ed Oxford: Elsevier Science Ltd, 2002, pp. 11-24.

[23] M. Nazmy, M. Staubli, G. Onofrio, and V. Lupinc, "Surface defect tolerance of a cast TiAl alloy in fatigue," *Scripta Materialia,* vol. 45, pp. 787-792, 2001.

Table 1 Chemical composition of the investigated alloys.

Alloy	Composition	Ti	Al	Nb	Mn	Cr	B	H	N	O
45XD	wt.%	Bal.	30.80	4.80	2.85	/	0.25	0.0023	0.0025	0.0640
	at.%	Bal.	44.70	2.02	2.03	/	0.91	0.0894	0.0070	0.1566
4622	wt.%	Bal.	32.00	4.90	/	2.65	0.05	0.0020	0.0045	0.0720
	at.%	Bal.	46.30	2.06	/	1.99	0.18	0.0775	0.0125	0.1757

Table 2. Tensile properties of 45XD and 4622 at room temperature.

Alloy	45XD							Alloy	4622			
No.	Tensile properties			No.	Tensile properties			No.	Tensile properties			
	$R_{p0.2}$ (MPa)	R_m (MPa)	A (%)		$R_{p0.2}$ (MPa)	R_m (MPa)	A (%)		$R_{p0.2}$ (MPa)	R_m (MPa)	A (%)	
1	539	611	0.71	31	541	610	0.68	1	493	509	0.33	
2	523	591	0.74	32	534	659	1.39	2	494	540	0.59	
3	-	505	0.10	33	524	659	1.52	3	483	589	1.50	
4	515	646	1.71	34	541	681	1.67	4	492	511	0.35	
5	527	647	1.33	35	535	672	1.68	5	493	551	0.74	
6	532	577	0.40	36	536	657	1.47	6	494	601	1.56	
7	524	638	1.31	37	504	624	1.38	7	-	496	0.18	
8	520	633	1.26	38	535	647	1.16	8	490	551	0.76	
9	544	648	0.97	39	533	655	1.42	9	487	576	1.15	
10	520	601	0.80	40	544	675	1.56	10	475	523	0.68	
11	523	597	0.66	41	539	616	0.68	11	489	589	1.37	
12	534	640	1.13	42	535	652	1.26	12	486	560	0.95	
13	532	641	1.11	43	537	638	1.04	13	508	600	1.28	
14	525	648	1.35	44	520	615	0.87	14	492	533	0.5	
15	543	658	1.29	45	528	639	1.22	15	493	521	0.39	
16	544	572	0.37	46	520	612	0.89	16	494	580	1.15	
17	517	537	0.31	47	537	665	1.37	17	481	591	1.49	
18	520	576	0.50	48	535	648	1.08	18	477	564	1.11	
19	509	567	0.50	49	523	594	0.62	19	487	589	1.34	
20	527	673	1.61	50	523	600	0.66	20	-	464	0.08	
21	530	666	1.62					21	486	538	0.58	
22	519	656	1.44					22	488	537	0.58	
23	525	666	1.55					23	487	535	0.56	
24	523	656	1.59					24	482	582	1.33	
25	522	643	1.35					25	487	526	0.43	
26	516	653	1.61					26	479	551	0.79	
27	520	647	1.40					27	487	572	0.98	
28	522	643	1.22					28	488	575	1.09	
29	518	651	1.39					29	490	577	1.11	
30	535	652	1.31					30	479	482	0.22	

$R_{p0.2}$: yield strength; R_m: ultimate strength; A: plastic strain.

Figure Captions:

Fig. 1. Microstructures of (a) 45XD and (b) 4622.

Fig. 2. 3D high resolution X-ray tomography results: (a) is the schematic diagram of the detection range, (b) shows inclusions observed in sample 4622-10 and (c) is the size distribution of inclusions in samples 4622-10 and 4622-11.

Fig. 3. Typical stress-strain curves of (a) 45XD and (b) 4622 with varying tensile properties.

Fig. 4. Fracture surfaces of 45XD. (a) Sample with no defects observed (sample 45XD-7: $R_{p0.2}$ = 524 MPa, R_m = 638 MPa, A = 1.31%); (b) sample failed from an yttria inclusion (sample 45XD-18: $R_{p0.2}$ = 520 MPa, R_m = 576 MPa, A = 0.50%), (c) being the magnified BSE image and (d) the EDS result of the inclusion; (e) sample failed from a 'facet' (lamella perpendicular to the loading axis), (f) being an enlarged image of the facet (sample 45XD-9: $R_{p0.2}$ = 544 MPa, R_m = 648 MPa, A = 0.97%).

Fig. 5. Categorization of yttria inclusions according to location and morphology: (a) surface/ agglomerate, (b) internal/ agglomerate, (c) surface/ whole piece, (d) internal/ whole piece. An agglomerate inclusion consists of segmented small yttria particles, and a whole piece inclusion consists of one big yttria particle.

Fig. 6. Tensile properties of 45XD (a, c, e) and 4622 (b, d, f) with different inclusion location and morphology against size.

Fig. 7. Fracture surfaces of a tensile test sample, with yttria inclusions observed on both halves of the fractured sample.

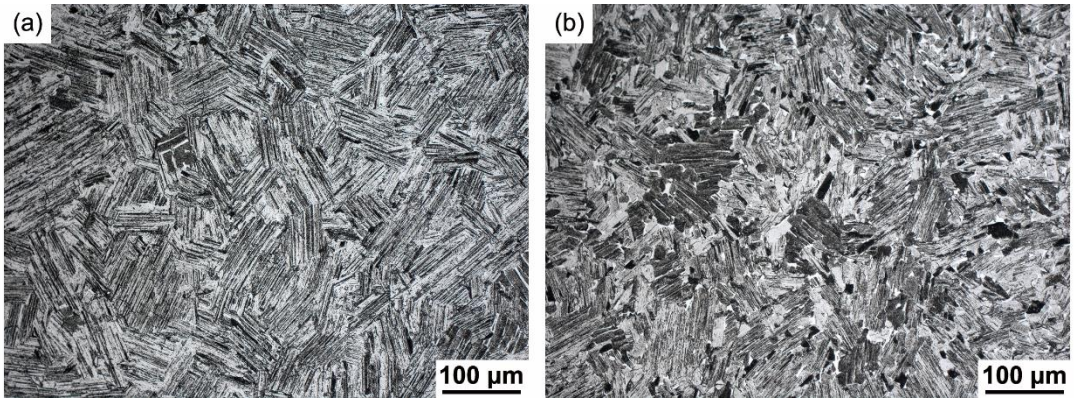

Fig. 1. Microstructures of (a) 45XD and (b) 4622.

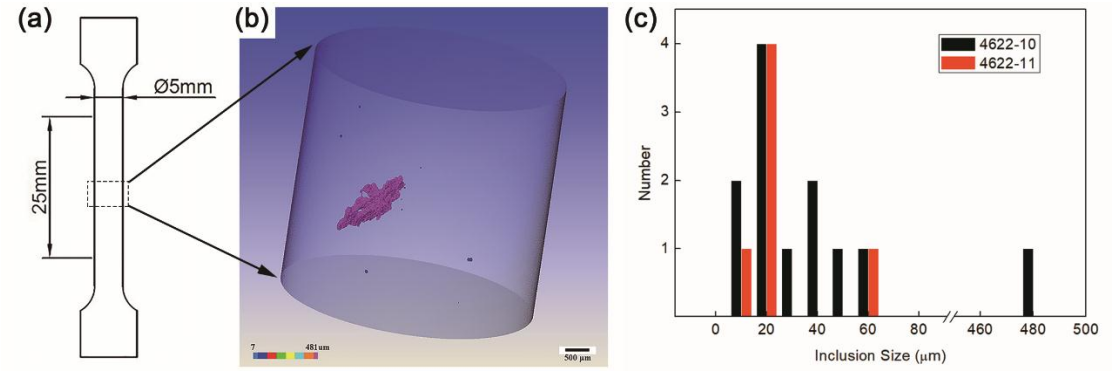

Fig. 2. 3D high resolution X-ray tomography results: (a) is the schematic diagram of the detection range, (b) shows inclusions observed in sample 4622-10 and (c) is the size distribution of inclusions in samples 4622-10 and 4622-11.

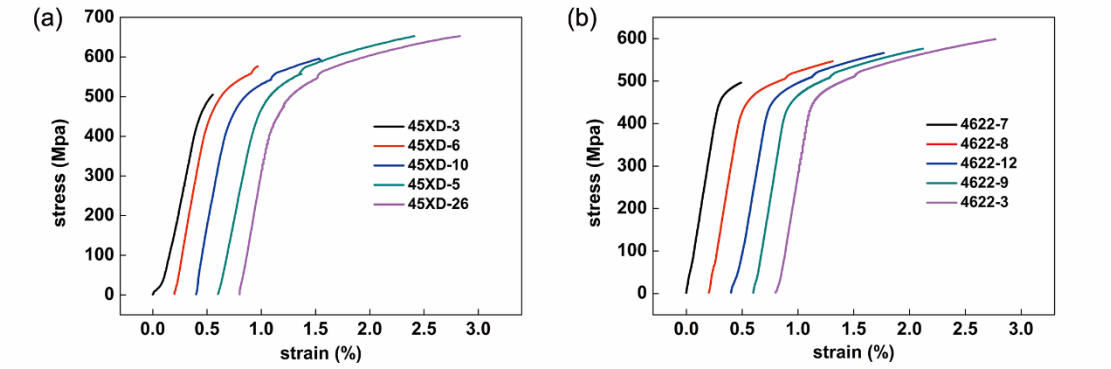

Fig. 3. Typical stress-strain curves of (a) 45XD and (b) 4622 with varying tensile properties.

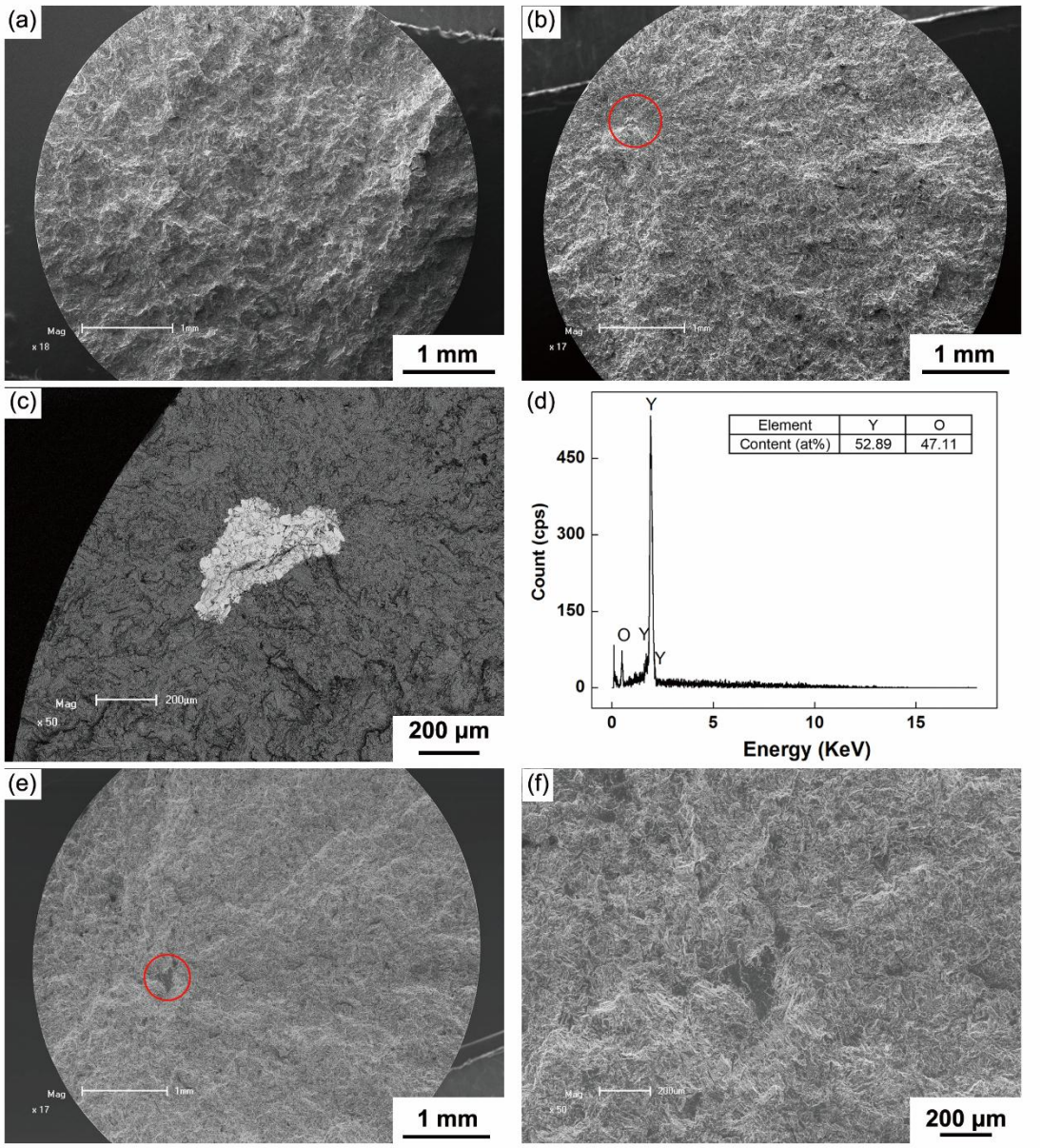

Fig. 4. Fracture surfaces of 45XD. (a) Sample with no defects observed (sample 45XD-7: $R_{p0.2}$ = 524 MPa, R_m = 638 MPa, A = 1.31%); (b) sample failed from an yttria inclusion (sample 45XD-18: $R_{p0.2}$ = 520 MPa, R_m = 576 MPa, A = 0.50%), (c) being the magnified BSE image and (d) the EDS result of the inclusion; (e) sample failed from a 'facet' (lamella perpendicular to the loading axis), (f) being an enlarged image of the facet (sample 45XD-9: $R_{p0.2}$ = 544 MPa, R_m = 648 MPa, A = 0.97%).

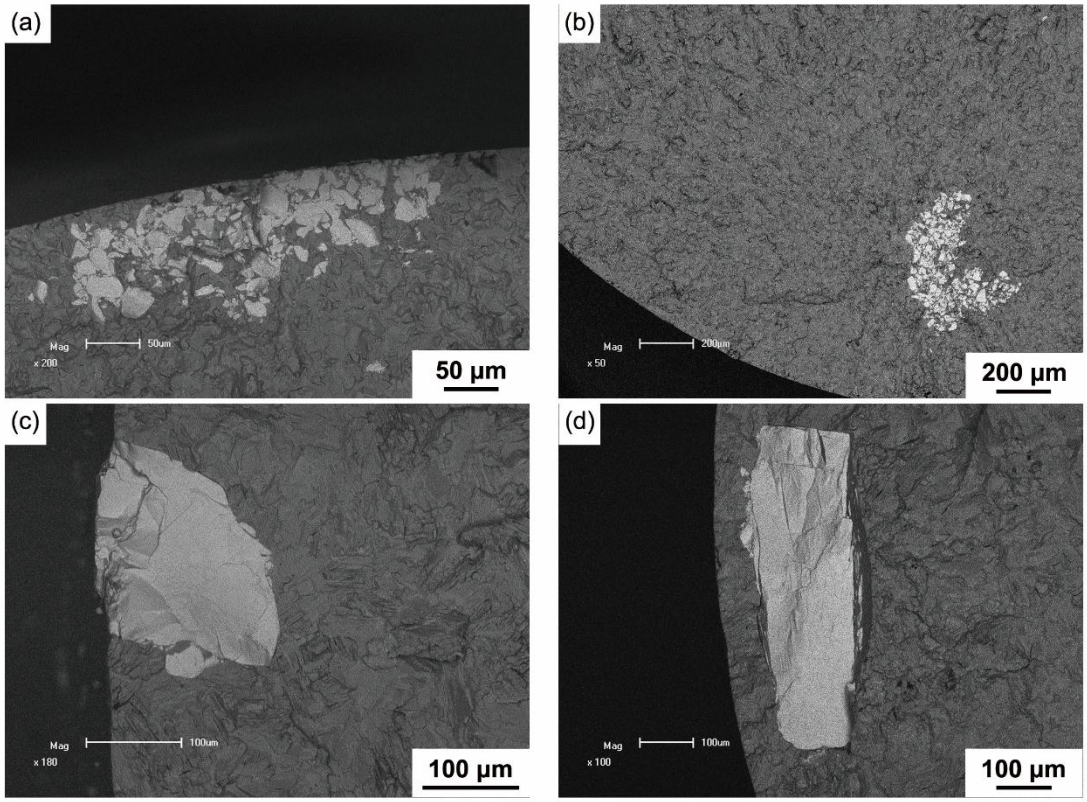

Fig. 5. Categorization of yttria inclusions according to location and morphology: (a) surface/ agglomerate, (b) internal/ agglomerate, (c) surface/ whole piece, (d) internal/ whole piece. An agglomerate inclusion consists of segmented small yttria particles, and a whole piece inclusion consists of one big yttria particle.

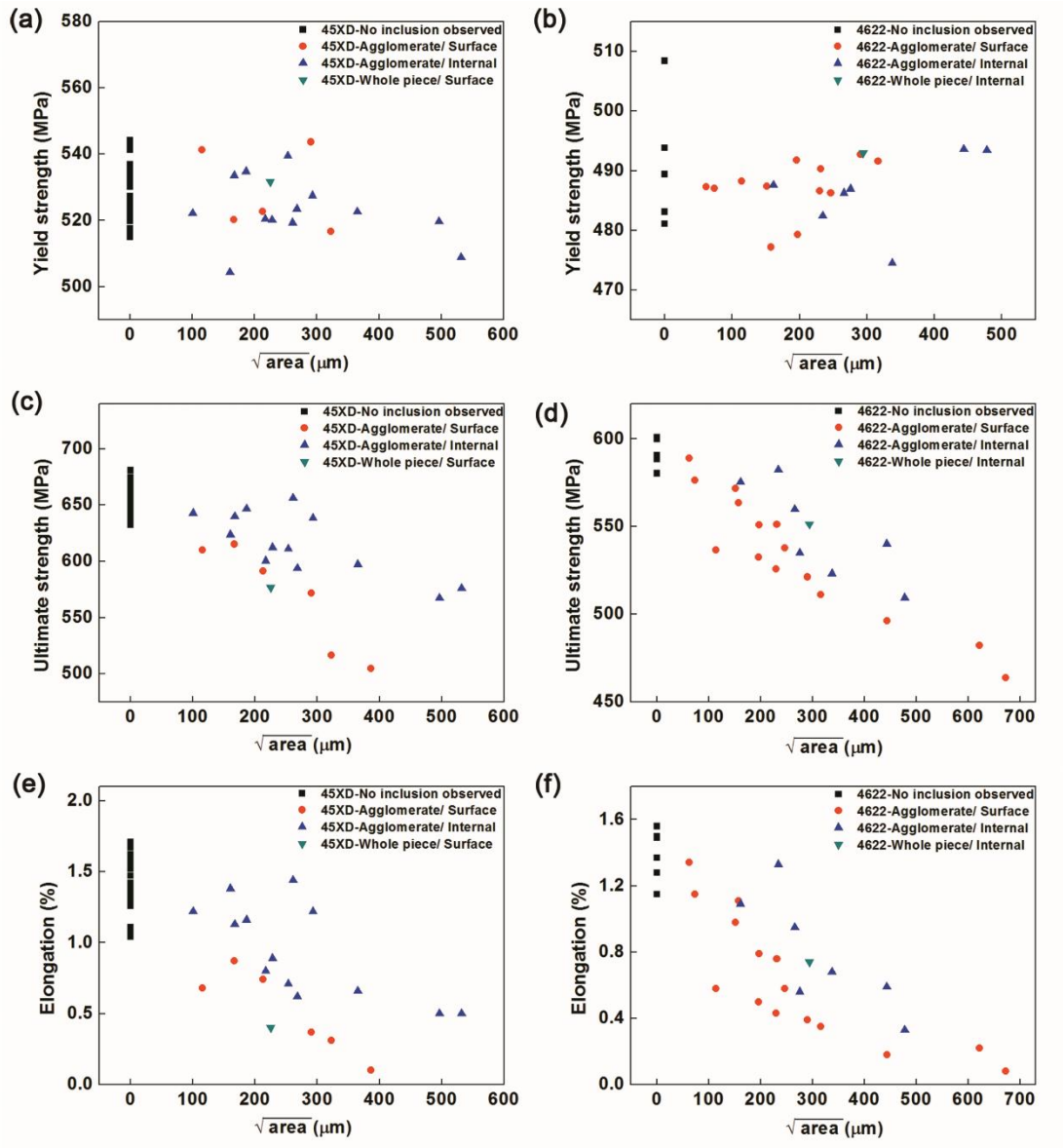

Fig. 6. Tensile properties of 45XD (a, c, e) and 4622 (b, d, f) with different inclusion location and morphology against size.

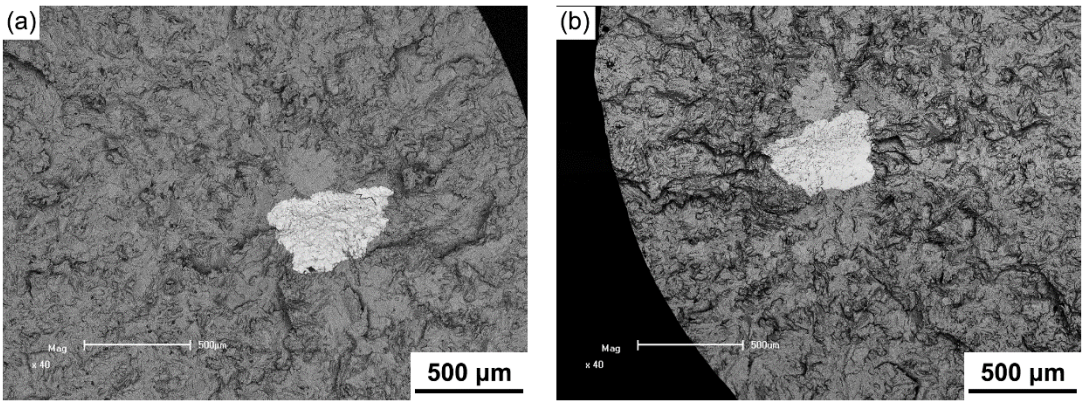

Fig. 7. Fracture surfaces of a tensile test sample, with yttria inclusions observed on both halves of the fractured sample.